Oral presentation | Turbulence simulation (DNS,LES,RANS)
Turbulence simulation(DNS,LES,RANS)-I
Wed. Jul 17, 2024 2:00 PM - 4:00 PM Room B

[8-B-04] Validating Quadratic Constitutive Relation using Flow Database at High Reynolds Numbers

*Yoshiharu Tamaki[1], Soshi Kawai[2], Taro Imamura[1] (1. The University of Tokyo, 2. Tohoku University)

Keywords: turbulence modeling, RANS, quadratic constitutive relation

©Retained by Authors

Validating Quadratic Constitutive Relation using Flow Database at High Reynolds Numbers

Yoshiharu Tamaki*, Soshi Kawai**, and Taro Imamura *
Corresponding author: ytamaki@g.ecc.u-tokyo.ac.jp
* The University of Tokyo, Japan.
** Tohoku University, Japan.

Keywords: Turbulence modeling, RANS, Turbulence constitutive relations.

1 Introduction

Anisotropy of Reynolds stress causes secondary flow motions in certain types of flows. Such secondary flow motions are called the second kind of Prandtl's secondary flow [1]. In order to predict the secondary flow motions, it is essential to incorporate the effects of anisotropy of the Reynolds stress into turbulence models. Among the anisotropic turbulence models, the quadratic constitutive relation proposed by Spalart [2] is one of the most popular models. QCR2000 defines the nonlinear relationship between the Reynolds stress and velocity gradient and can be used with any baseline turbulence model based on the eddy-viscosity assumption. Due to the simplicity of its formulation, QCR2000 has been used widely in engineering applications. Nevertheless, since QCR2000 is calibrated only in a square duct flow, the validity of its parameter constant (C_{cr1}) is still arguable.

Most recently, the authors [3] have developed a modified quadratic constitutive relation (hereafter denoted as QCR2024) by analyzing the relationship between the Reynolds stress and mean velocity field in a sidewall interference flow. Like QCR2000, QCR2024 can be used with any baseline turbulence model based on the eddy-viscosity assumption because its formulation does not contain variables specific to the turbulence model. The previous study [3] showed that QCR2024 predicts the turbulence anisotropy and resulting corner-flow separation better than QCR2000. Therefore, in this study, we further investigate the validity and robustness of QCR2024 using databases from large-eddy simulations (LES) of several different types of flows, a near-stall airfoil flow [4], a separating-reattaching boundary layer [5], and the entire 3D flow around a high-lift configuration aircraft [6].

2 Numerical methods

2.1 QCR2024 formulation

QCR2024 models the Reynolds stress as

$$-\overline{u_i' u_j'} = 2\nu_t \hat{S}_{ij} - \frac{2}{3} K \delta_{ij}, \tag{1}$$

where

$$\hat{S}_{ij} = \left[S_{ij} - \frac{C_{q1}}{\|\mathbf{u_x}\|}(S_{ik}\Omega_{jk} + S_{jk}\Omega_{ik}) - \frac{C_{q2}}{\|\mathbf{u_x}\|}\left(S_{ik}S_{jk} - \frac{1}{3} S_{mn}S_{mn}\delta_{ij} \right) \right], \; K = \frac{3}{2}\nu_t C_k \sqrt{2\Omega_{mn}\Omega_{mn}},$$

$$S_{ij} \equiv \frac{1}{2}\left(\frac{\partial u_i}{\partial x_j} + \frac{\partial u_j}{\partial x_i} \right), \; \Omega_{ij} \equiv \frac{1}{2}\left(\frac{\partial u_i}{\partial x_j} - \frac{\partial u_j}{\partial x_i} \right), \; \|\mathbf{u_x}\| \equiv \sqrt{\frac{\partial u_m}{\partial x_n}\frac{\partial u_m}{\partial x_n}}.$$

Here, u_i is the velocity vector, x_i is the coordinate, ν_t is the eddy viscosity, and $K \equiv \overline{u_i' u_i'}/2$ is the turbulent kinetic energy. C_{q1} and C_{q2} determine the strength of anisotorpy, while C_k determines the magnitude of turbulence kinetic energy. Our previous study [3] determined these parameters based on

the LES data of a sidewall interference flowfield as $(C_{q1},\ C_{q2},\ C_k) = (1.0,\ 0.5,\ 2.15)$, which are found to be almost globally valid in that flowfield except for the inner layer of the turbulent boundary layer. Note that if the parameters are $(C_{q1},\ C_{q2},\ C_k) = (0.6,\ 0.0,\ 0.0)$, Eq. (1) is reduced to QCR2000 [2]. Also, $(C_{q1},\ C_{q2},\ C_k) = (0.0,\ 0.0,\ 0.0)$ recovers a linear constitutive relation (LCR), i.e., Boussinesq's eddy viscosity approximation.

2.2 Validation methodology

As in our previous study [3], we investigate the validity of the parameters C_{q1} and C_{q2} by evaluating the alignment between R_{ij} and $\hat{S}_{ij}$ as

$$\sigma \equiv \frac{R_{ij}\hat{S}_{ij}}{\sqrt{R_{ij}R_{ij}}\sqrt{\hat{S}_{ij}\hat{S}_{ij}}}. \tag{2}$$

where $R_{ij} \equiv -\overline{u_i'u_j'} + 2/3K\delta_{ij}$ is the deviatoric part of the Reynolds stress tensor. σ indicates the alignment between the tensors R_{ij} and $\hat{S}_{ij}$, which ranges from -1 to 1. $\sigma = 1$ means the deviatoric part is perfectly reproduced by introducing a proper positive scalar eddy viscosity. In the following, R_{ij} and $\hat{S}_{ij}$ are computed from the statistically averaged flowfield obtained by the LES.

3 Results

3.1 Near-stall airfoil flow

First, the validity of QCR2024 is examined in a near-stall airfoil flow at a high Reynolds number. We employ the data from the wall-resolved LES around the Aerospatial A-airfoil [4], whose data are available on website [7]. In this LES, Re_c, the Reynolds number based on the chord length c and the freestream velocity u_∞, is 1.0×10^7. Also, the freestream Mach number is 0.15, and the angle of attack α is 13.3 degrees. Figure 1 shows the isosurfaces of the Q criterion around the airfoil. The boundary layer over the upper airfoil surface experiences transition to turbulence at $x/c \approx 0.1$ and develops along the airfoil surface. The boundary layer forms a thickened shear layer downstream, while the mean flow at the trailing edge remains attached.

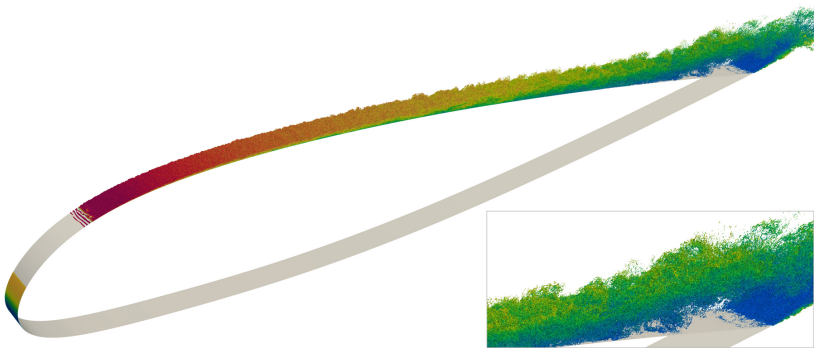

Figure 1: Isosurfaces of Q criterion colored by the stream velocity in the LES around the airfoil [4].

Figure 2 shows the distributions of σ near the airfoil calculated by QCR2024, QCR2000, and LCR using Eq. (2). Also, Fig. 3 compares the profiles of σ and TKE at two locations over the upper airfoil surface ($x/c = 0.3$ and 0.9). QCR2024 yields higher values of σ than QCR2000 and LCR, except in the lower part of the wake. When using QCR2024, σ is mostly higher than 0.98 in the near-wall region, meaning that QCR2024 accurately reproduces the anisotropy of the Reynolds stress in the turbulent boundary layer.

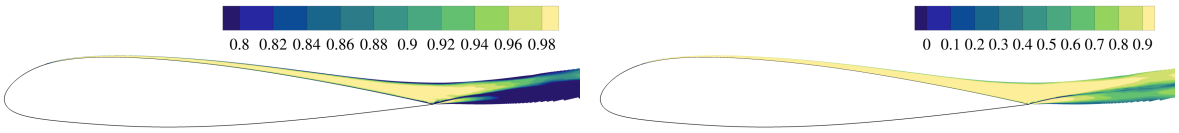

(a) QCR2024

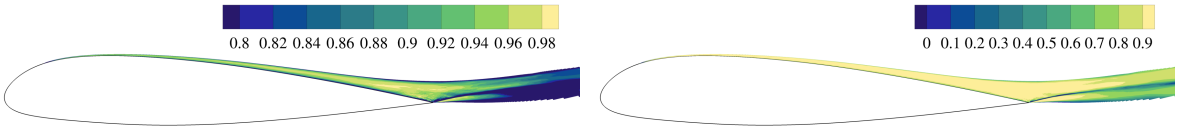

(b) QCR2000

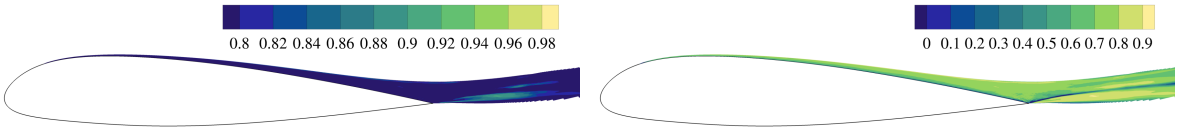

(c) Boussinesq approximation

Figure 2: Distributions of σ in the near-stall airfoil flowfield. Only the regions with $K/u_\infty^2 > 10^{-3}$ are shown. Left and right figures differ only in the contour range.

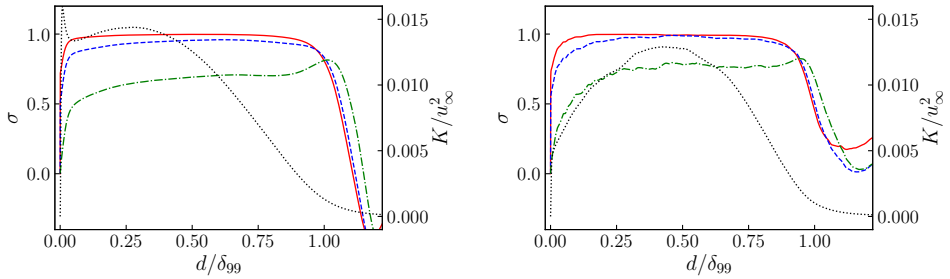

(a) $x/c = 0.3$ (upper surface)

(b) $x/c = 0.9$ (upper surface)

Figure 3: Profiles of σ in the near-stall airfoil flowfield, where ——, QCR2024; - - -, QCR2000, —·—, LCR; ·····, TKE (using the right axis).

3.2 Separating and reattaching boundary layer

Next, we investigate the validity of QCR2024 in the separating and reattaching boundary layer. For this case, we employ the database from the wall-resolved LES conducted by Kamogawa *et al.* [5, 7] (see Fig. 4). Here, the inflow turbulent boundary layer is generated by the rescaling-reintroducing method [8]. The Reynolds number based on the momentum thickness and the boundary layer edge velocity is approximately 2.0×10^3, and the free-stream Mach number is 0.2. The boundary layer separates at $x/\theta_0 \approx 130$ and reattaches at $x/\theta_0 \approx 250$ due to the suction and blowing subscribed at the top computational boundary.

Figure 5 compares the distribution of σ calculated by QCR2024, QCR2000, and LCR. QCR2024 yields overall high σ values, except for the near-wall region after the flow reattachment. The decrease of σ in this region is assumed to be because of the large-scale streamwise elongated structures near the reattachment (see Abe [9]). Although further consideration is desirable for this point, the results reconfirm that QCR2024 is applicable to the attached turbulent boundary layers under an adverse pressure gradient.

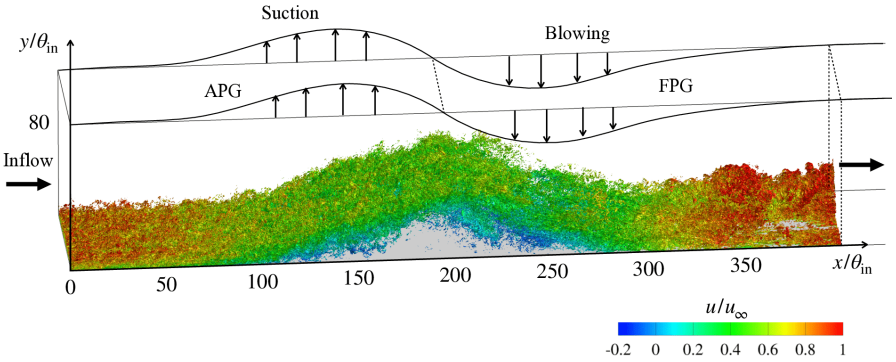

Figure 4: Isosurfaces of Q criterion colored by the stream velocity in the LES of the separating and reattaching boundary layer [5].

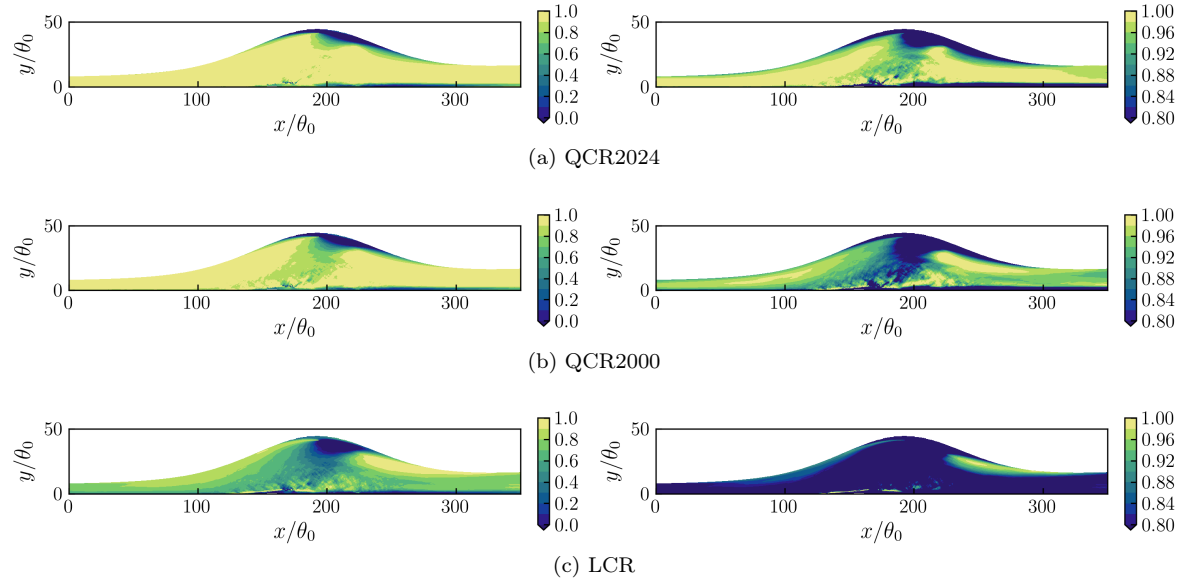

Figure 5: Distributions of σ in the separating and reattaching boundary layer. Only the regions with $K/u_\infty^2 > 10^{-3}$ are shown. Left and right figures differ only in the contour range.

3.3 Flow around a high-lift aircraft

As a demonstration in a more complex flowfield, we investigate the flow around an entire high-lift aircraft configuration. Here, the target is the low-speed flow around the JAXA standard model (JSM) [10]. The JSM is a high-lift aircraft model consisting of fuselage, wing, slat, and flap, where the mean aerodynamic chord (MAC) is 529.2mm. The validation database is taken from the wall-modeled LES conducted by Asada *et al.* [6]. The Reynolds number based on the MAC and freestream velocity is 1.93×10^6, and the freestream Mach number is 0.172. Figure 6 shows the iso-surfaces of the Q criterion colored by the streamwise velocity. Here, most of the upper wing surface is covered by turbulent vortices, where some visible large structures (e.g., the wakes from the slat support brackets and nacelle) are also observed.

Figure 7 shows the distribution of σ over the streamwise and spanwise cross-planes. Also, Fig. 8 shows the close-up view of the wing-body junction with a narrower contour range. Though not shown here, the QCR2000 result falls roughly between the QCR2024 and LCR results. Although the results contain significant noise due to the shortage of the averaging period, QCR2024 yields overall higher σ values in the near-body region. In particular, QCR2024 shows improvement over LCR near the wing-body junction in Fig. 8, near the fuselage in Fig. 7 (a, b), and over the upper wing surface in Fig. 7 (c).

The results also suggest the difficulty in modeling the off-body region, e.g., the nacelle wake (the region between the fuselage and wing in Fig. 7 (a, b)). In the off-body region, the Reynolds stress contains the contributions of both turbulence and large-scale oscillating motions. Indeed, a large-scale

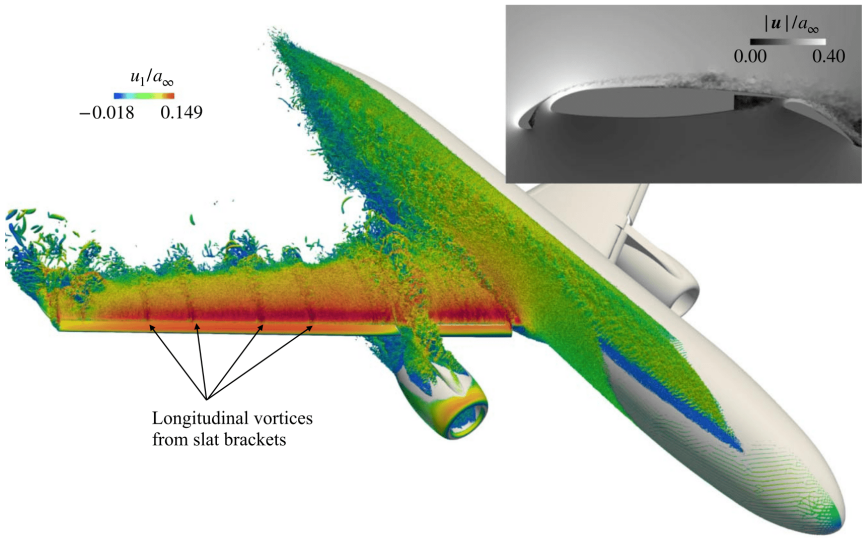

Figure 6: Instantaneous iso-surfaces of Q criterion colored by streamwise velocity and velocity magnitude at 56.5% spanwise cross section (inset) [6].

helical structure is observed from the nacelle upper surface, as shown in Fig. 6. It seems challenging to model the Reynolds stress due to the large-scale structure using the gradient of the mean flow velocity, as in the present QCR modeling. Hence, scale-resolving (i.e., RANS-LES hybrid) simulations may be more suitable for this flowfield because they can avoid modeling the large-scale motions. Nevertheless, the present modeling will also improve the prediction of the near-wall part, which must be modeled even in scale-resolving simulations.

4 Conclusions

The latest quadratic constitutive relation (QCR2024) is validated using the databases from large-eddy simulations (LES) at high Reynolds numbers. For the validation of the deviatoric part, the alignment between the traceless Reynolds stress tensor and the strain-like tensor defined by the QCR is calculated. In all the examined cases, QCR2024 yields better tensor alignment in the near-wall region, including the adverse pressure gradient boundary layer and near-body part of the wake, than the linear eddy viscosity approximation (LCR) or the existing quadratic constitutive relation (QCR2000). This result means that QCR2024 accurately reproduces the anisotropy of the Reynolds stress in the boundary layer. On the other hand, the results also suggest the challenges in the modeling. First, the near-wall part of the boundary layer immediately after the reattachment is not modeled accurately in QCR2024. Second, in the off-wall regions, such as the wake, the modeling becomes difficult because the Reynolds stress contains the contribution of the large-scale flow motions. Although treatments for these challenges are desirable for further improvement, the present validation study suggests that QCR2024 is promising for its primary target, i.e., prediction of the corner-flow separation at the wing-body junction.

Further analysis of the modeling, such as the validation of C_k, will be presented in [11].

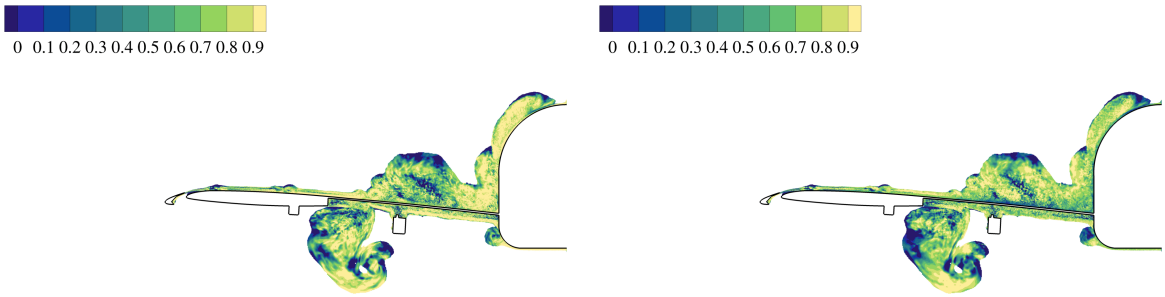

(a) $x = 2600$ mm

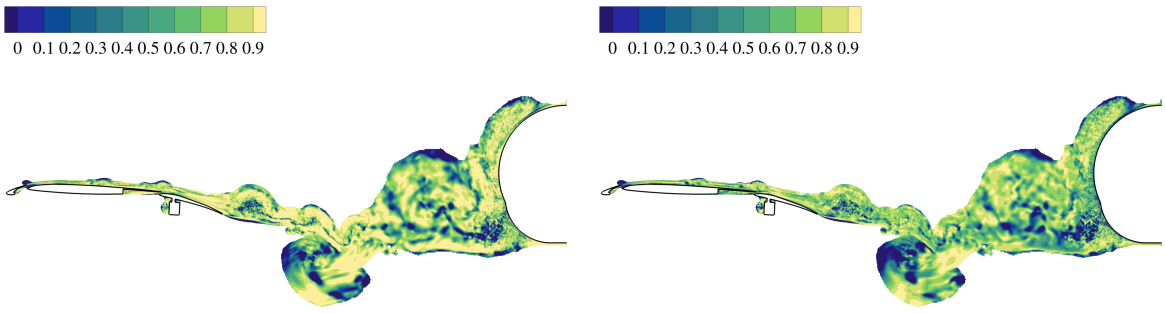

(b) $x = 3000$ mm

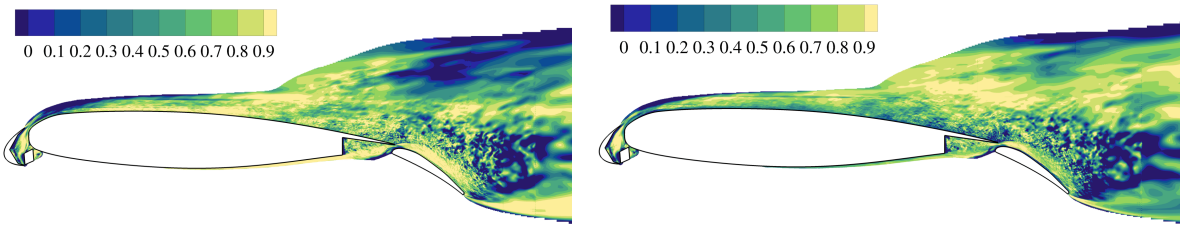

(c) $y = 460$ mm

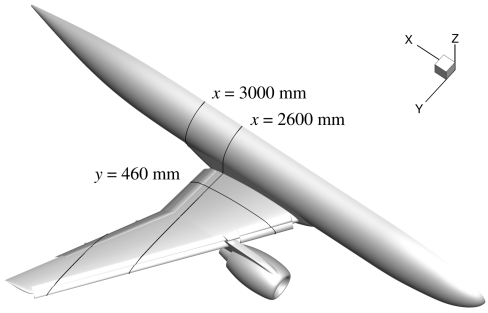

(d) Definition of cross-planes

Figure 7: Distribution of σ over the cross-planes around the JSM. Left, QCR2024, right, LCR. Only the regions with $K/u_\infty^2 > 10^{-3}$ are shown.

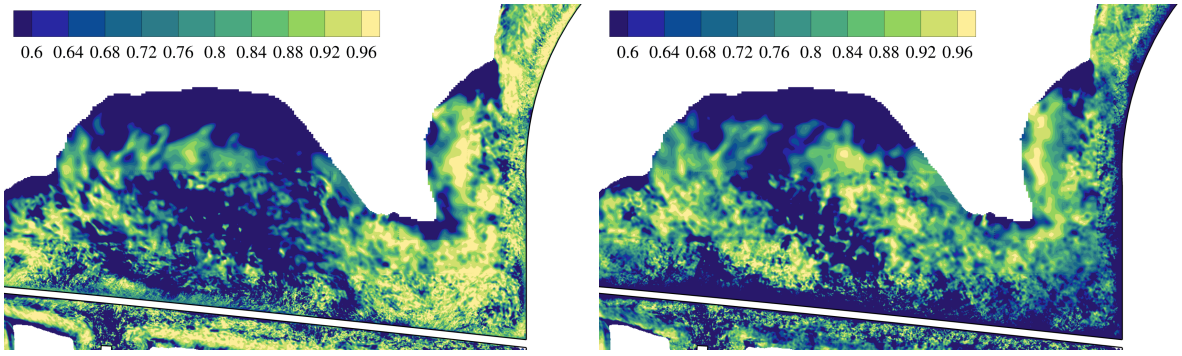

Figure 8: Close-up view of the σ distribution near the wing-body junction at $x = 2600$ mm. Left, QCR2024, right, LCR.

Acknowledgment

This work was supported in part by the Japan Society for the Promotion of Science (JSPS) Grant-in-Aid for Young Scientists (Start-up) JP20K22379. SK was supported in part by the Ministry of Education, Culture, Sports, Science and Technology (MEXT) as "Program for Promoting Researches on the Supercomputer Fugaku (Leading research on innovative aircraft design technologies to replace flight test, JPMXP1020200312; and Research toward DX in aircraft development led by digital flight, JPMXP1020230320) by Japan with computer resources awarded by the supercomputer Fugaku provided by RIKEN Center for Computational Science (Project ID: hp200137, hp210168, hp220160, hp230197, hp240203). The authors acknowledge Dr. Asada of Tohoku University, who handled and provided the statistical data of the flow around JSM.

References

[1] P. Bradshaw. Turbulent secondary flows. *Annual Review of Fluid Mechanics*, 19(1):53–74, 1987.
[2] P. R. Spalart. Strategies for turbulence modelling and simulations. *International Journal of Heat and Fluid Flow*, 21(3):252–263, 2000.
[3] Y. Tamaki and S. Kawai. Turbulence anisotropy effects on corner-flow separation: physics and turbulence modeling. *Journal of Fluid Mechanics*, 980:A21, 2024.
[4] Y. Tamaki and S. Kawai. Wall-resolved large-eddy simulation of near-stall airfoil flow at $Re_c = 10^7$. *AIAA Journal*, 61(2):698–711, 2023.
[5] R. Kamogawa, Y. Tamaki, and S. Kawai. Ordinary-differential-equation-based nonequilibrium wall modeling for large-eddy simulation. *Physical Review Fluids*, 8(6):064605, 2023.
[6] H. Asada, Y. Tamaki, R. Takaki, T. Yumitori, S. Tamura, K. Hatanaka, K. Imai, H. Maeyama, and S. Kawai. FFVHC-ACE: fully automated Cartesian-grid-based solver for compressible large-eddy simulation. *AIAA Journal*, 61(8):3466–3484, 2023.
[7] `https://www.klab.mech.tohoku.ac.jp/database/index.html`. (Retrieved on June 14th, 2024).
[8] G. Urbin and D. Knight. Large-eddy simulation of a supersonic boundary layer using an unstructured grid. *AIAA Journal*, 39(7):1288–1295, 2001.
[9] H. Abe. Reynolds-number dependence of wall-pressure fluctuations in a pressure-induced turbulent separation bubble. *Journal of Fluid Mechanics*, 833:563–598, 2017.
[10] Y. Yokokawa, M. Murayama, H. Uchida, K. Tanaka, T. Ito, and K. Yamamoto. Aerodynamic influence of a half-span model installation for high-lift configuration experiment. In *48th AIAA Aerospace Sciences Meeting Including the New Horizons Forum and Aerospace Exposition*, 2010. AIAA Paper No. 2010-0684.
[11] Y. Tamaki, S. Kawai, and T. Imamura. Reynolds stress constitutive relations in high Reynolds number large-eddy simulation databases. (in preparation).